

# The relativistic G-matrix approach and applications

Rolf Brockmann

*Institute of Physics, University of Mainz, Germany*

The Dirac-Brueckner approach to the nuclear many-body problem is described. A family of relativistic meson-exchange potentials is used which apply the pseudovector coupling for the interaction of pseudoscalar mesons ( $\pi$ ,  $\eta$ ) with nucleons. These potentials describe low-energy two-nucleon scattering and the deuteron data accurately. Using these potentials, the properties of nuclear matter are calculated in the Dirac-Brueckner-Hartree-Fock approximation, in which the empirical nuclear matter saturation is explained quantitatively. Size and nature of relativistic effects included in the present approach are examined in detail. Furthermore the relativistic density-dependent Hartree approximation is applied for finite nuclei, where the coupling constants of the relativistic Hartree-Lagrangian are made density dependent and are obtained from the relativistic Brueckner-Hartree-Fock results of nuclear matter. The calculated results on binding energies and root mean square radii of  $^{16}\text{O}$  and  $^{40}\text{Ca}$  agree well with experiment. The charge densities from electron scattering are also calculated and their dependence on the nucleon-nucleon interaction is discussed in relation with nuclear matter properties.

## 1. NN-interaction

In the early nineties S. Weinberg wrote three famous papers on nuclear forces from chiral Lagrangians.<sup>1)</sup> He used the most general possible Lagrangian involving pions and low-energy nucleons consistent with spontaneously broken chiral symmetry and other known symmetries. The potential between two nucleons can be determined using Feynman diagram techniques. Looking at NN-scattering with momenta lower than  $Q$  ( $Q \leq m_N$ ) it is possible to expand the potential between two nucleons in terms of increasing order in  $Q$  and  $m_\pi$ . This famous power counting scheme guarantees that terms with higher order in  $Q$  and/or  $m_\pi$  are less important for the two-body potential.

Recently D. B. Kaplan, M. J. Savage, and M. B. Wise<sup>2)</sup> argued that it may be more appropriate to expand the S-matrix and not the potential. Following their arguments we shall also find an answer to the question: Why is there no simple (perturbation) theory for nuclei? At a first glance it is very amazing that nuclei cannot be understood within the framework of a perturbation theory since single particle energies of nucleons inside a nucleus are very small compared to the nucleon mass. The ratio is about 5%. The same is true for single particle potentials. Now let us sketch their approach for NN scattering since it leads us naturally to *ladder diagrams*.

For s-waves the scattering amplitude  $\mathcal{A}$  is related to the phase shift  $\delta$  by

$$\mathcal{A} = \frac{4\pi}{M} \frac{1}{p \cos \delta - ip}, \quad (1)$$

where  $M$  is the nucleon mass and  $p$  the magnitude of the 3-momentum of each nucleon in the center of mass frame.

It is well-known from elementary quantum mechanics that the quantity  $p \cot \delta$  and not  $\mathcal{A}$  has a nice momentum expansion for  $p \leq \Lambda (\sim M)$ .

$$p \cot \delta = -\frac{1}{a} + \frac{1}{2} \Lambda^2 r_0 \frac{p^2}{\Lambda^2} + \dots, \quad (2)$$

where  $a$  is the scattering length and  $r_0$  is the effective range. The expression in Eq. (2) is the so-called effective range expansion. If the low-energy parameters are of natural size ( $|a| \sim \frac{1}{\Lambda}$  and  $|r_0| \sim \frac{1}{\Lambda}$ ), then there is a simple momentum expansion of the scattering amplitude:

$$\mathcal{A} = -\frac{4\pi a}{M} (1 - iap + (ar_0/2 - a^2)p^2 + \dots). \quad (3)$$

This amplitude is a power series in the momentum  $p$  and consecutive terms are getting smaller

$$\mathcal{A} = \sum_{n=0}^{\infty} \mathcal{A}_n \quad \text{and} \quad \mathcal{A}_n \sim \mathcal{O}(p^n). \quad (4)$$

The situation is different for NN scattering since the scattering length is very large ( $\sim 23$  fm). In this case the expansion has to be done in a different way:

$$\mathcal{A} = -\frac{4\pi}{M} \frac{1}{(1/a + ip)} \left(1 + \frac{r_0/2}{1/a + ip} + \dots\right). \quad (5)$$

$1/a$  is a small quantity. Therefore the leading order term is proportional to  $p^{-1}$ :

$$\mathcal{A} = \sum_{n=-1}^{\infty} \mathcal{A}_n \quad \text{and} \quad \mathcal{A}_n \sim \mathcal{O}(p^n). \quad (6)$$

In the following we show how to treat this nontrivial case in the framework of field theory. An effective field theory of interacting nucleons has been formulated in the above mentioned papers by Weinberg:

$$\begin{aligned} \mathcal{L}_{eff} = & N^+ (i\partial_t + \nabla^2/2M) N \\ & + [C_0(N^+N)^2 + C_2[(NN)^+(N \overleftrightarrow{\nabla}^2 N) + h.c.] + \dots]. \quad (7) \end{aligned}$$

The first and the second term in the second line of this Lagrangian corresponds to the left and right term of Fig. 1, respectively.

Using an appropriate regularization scheme (the so-called power divergence subtraction of Kaplan, Savage and Wise<sup>2)</sup>)

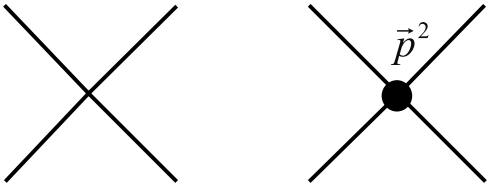


Fig. 1. Interaction terms of the Lagrangian.

the amplitude of Eq. (7) can be calculated term by term. In Fig. 2 the Feynman diagrams of the lowest order terms are displayed. In the next step pions have to be included. Of course Weinberg included pions in his papers. At this point we would like to make contact to our own work.<sup>3)</sup> We started from an effective chiral  $\pi$ N-Lagrangian up to order  $q^0$  and  $q^1$  and worked out the corresponding NN-potential. Only the first diagram of Fig. 3 leads to the one-pion-exchange while the one-loop corrections only contribute to mass and coupling constant renormalization.

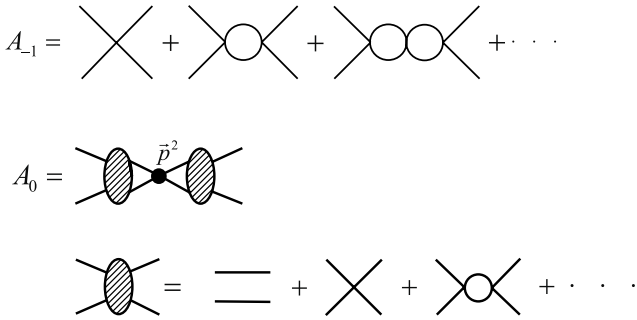


Fig. 2. Lowest order terms of the NN-scattering amplitude Eq. (5) using the Lagrangian Eq. (7).

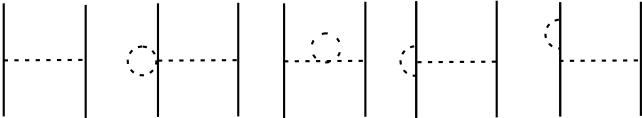


Fig. 3. Lowest order diagrams which contribute to the one-pion-exchange.

Then we worked out the two-pion-exchange diagrams of Fig. 4 and diagrams which involve  $\Delta$ -degrees of freedom. Let us summarize our results:

- (1) Phase shifts up to 350 MeV laboratory energy are reproduced for  $L \geq 3$ .
- (2) The strength of the empirical central potential is reproduced!
- (3) The empirical spin-orbit potential is reproduced for  $r \geq 1$  fm!

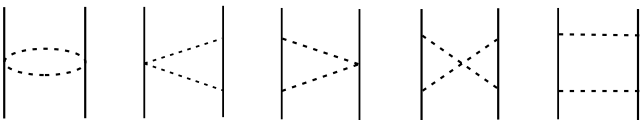


Fig. 4. Two-pion-exchange diagrams contributing to the NN-force.

This looks very promising. A difficult and important part for the future will be to combine the short-range part of the NN-interaction (Eq. (7)) with the long-range one-pion-exchange and the intermediate two-pion-exchange within a rigorous field theoretic treatment including Weinberg's power counting and dimensional regularization of ultra-violet divergences!

Furthermore we learned from this introduction that we need to iterate the short-range part of the NN-interaction to all orders (see Fig. 2) to obtain the unusual large scattering length. The corresponding procedure for OBEPs (One-Boson-Exchange Potentials) is the ladder approximation which will be solved using the Thompson or Blankenbecler-Sugar equation.

## 2. The Dirac-Brueckner approach

The essential point of the Dirac-Brueckner approach is to use the Dirac equation for the single-particle motion in nuclear matter

$$(\not{p} - M - U)\tilde{u}(\mathbf{p}, s) = 0, \quad (8)$$

or in Hamiltonian form

$$(\boldsymbol{\alpha} \cdot \mathbf{p} + \beta M + \beta U)\tilde{u}(\mathbf{p}, s) = \epsilon_p \tilde{u}(\mathbf{p}, s), \quad (9)$$

with

$$U = U_S + \gamma^0 U_V, \quad (10)$$

where  $U_S$  is an attractive scalar and  $U_V$  (the time-like component of) a repulsive vector field. (Notation as in the book of Bjorken and Drell;<sup>4)</sup>  $\beta = \gamma^0$ ,  $\alpha^l = \gamma^0 \gamma^l$ .)  $M$  is the mass of the free nucleon.

The fields,  $U_S$  and  $U_V$ , are in the order of several hundred MeV and strongly density dependent. In nuclear matter they can be determined self-consistently. The resulting fields are in close agreement with those obtained in the Dirac phenomenology of scattering.

The solution of Eq. (8) is

$$\tilde{u}(\mathbf{p}, s) = \sqrt{\frac{\tilde{E}_p + \tilde{M}}{2\tilde{M}}} \begin{pmatrix} 1 \\ \frac{\boldsymbol{\sigma} \cdot \mathbf{p}}{\tilde{E}_p + \tilde{M}} \end{pmatrix} \chi_s, \quad (11)$$

with

$$\tilde{M} = M + U_S, \quad (12)$$

$$\tilde{E}_p = \sqrt{\tilde{M}^2 + \mathbf{p}^2}, \quad (13)$$

and  $\chi_s$  a Pauli spinor. The covariant normalization is  $\tilde{u}(\mathbf{p}, s)\tilde{u}(\mathbf{p}, s) = 1$ . Notice that the Dirac spinor Eq. (11) is obtained from the free Dirac spinor by replacing  $M$  by  $\tilde{M}$ .

As in conventional Brueckner theory, the basic quantity in the Dirac-Brueckner approach is a  $G$ -matrix, which satisfies an integral equation. In this relativistic approach, a relativistic

tic three-dimensional equation is chosen. Following the basic philosophy of traditional Brueckner theory, this equation is applied to nuclear matter in strict analogy to free scattering.

Including the necessary medium effects, the Thompson equation in the nuclear matter rest frame reads

$$\begin{aligned} \tilde{G}(\mathbf{q}', \mathbf{q}|\mathbf{P}, \tilde{z}) &= \tilde{V}(\mathbf{q}', \mathbf{q}) \\ &+ \int \frac{d^3k}{(2\pi)^3} \tilde{V}(\mathbf{q}', \mathbf{k}) \frac{\tilde{M}^2}{\tilde{E}_{\frac{1}{2}\mathbf{P}+\mathbf{k}}^2} \frac{Q(\mathbf{k}, \mathbf{P})}{\tilde{z} - 2\tilde{E}_{\frac{1}{2}\mathbf{P}+\mathbf{k}}} \tilde{G}(\mathbf{k}, \mathbf{q}|\mathbf{P}, \tilde{z}), \end{aligned} \quad (14)$$

with

$$\tilde{z} = 2\tilde{E}_{\frac{1}{2}\mathbf{P}+\mathbf{q}}. \quad (15)$$

$\mathbf{P}$  is the c.m. momentum, and  $\mathbf{q}, \mathbf{k}$  and  $\mathbf{q}'$  are the initial, intermediate and final relative momenta, respectively, of the two particles interacting in nuclear matter. The Pauli operator  $Q$  projects onto unoccupied states. In Eq. (14) we suppressed the  $k_F$  dependence as well as spin (helicity) and isospin indices. For  $|\frac{1}{2}\mathbf{P} \pm \mathbf{q}|$  and  $|\frac{1}{2}\mathbf{P} \pm \mathbf{k}|$  the angle average is used.

The energy per nucleon in nuclear matter, which is the objective of these calculations, is considered in the nuclear matter rest frame. Thus, the  $G$ -matrix is needed for the nuclear matter rest frame. Equation (14) gives this nuclear matter  $G$ -matrix directly in that rest frame. Alternatively, one can calculate the  $G$ -matrix first in the two-nucleon center-of-mass (c.m.) system (as customary in calculations of the  $T$ -matrix in two-nucleon scattering), and then perform a Lorentz transformation to the rest frame. This method<sup>5)</sup> is, however, complicated, involved, and cumbersome. The advantage of our procedure is that it avoids this complication. Further treatments of Eq. (14) can follow the lines established from conventional Brueckner theory, as e. g. the use of the angle averaged Pauli projector etc.. Numerically the equation can be solved by standard methods of momentum space Brueckner calculations.<sup>6)</sup>

The essential difference to standard Brueckner theory is the use of the potential  $\tilde{V}$  in Eq. (14). Indicated by the tilde, this meson-theoretic potential is evaluated by using the spinors of Eq. (11) instead of the free spinors applied in scattering as well as in conventional ('non-relativistic') Brueckner theory. Since  $U_S$  (and  $\tilde{M}$ ) are strongly density dependent, so is the potential  $\tilde{V}$ .  $\tilde{M}$  decreases with density. The essential effect in nuclear matter is a suppression of the (attractive)  $\sigma$ -exchange; this suppression increases with density, providing additional saturation. It turns out (see figures below) that this effect is so strongly density-dependent that *the empirical saturation and incompressibility* can be reproduced. Furthermore, the prediction for the Landau parameter  $f_0$  is considerably improved without deteriorating the other parameters. Note, that sum rules require  $f_0 > -1$  at nuclear matter density.<sup>7)</sup>

The single-particle potential

$$U(m) = \frac{\tilde{M}}{\tilde{E}_m} \langle m|U|m \rangle = \frac{\tilde{M}}{\tilde{E}_m} \langle m|U_S + \gamma^0 U_V|m \rangle$$

$$= \frac{\tilde{M}}{\tilde{E}_m} U_S + U_V, \quad (16)$$

is the self-energy of the nucleon which is defined in terms of the  $G$ -matrix formally in the usual way

$$U(m) = \text{Re} \sum_{n \leq k_F} \frac{\tilde{M}^2}{\tilde{E}_n \tilde{E}_m} \langle mn|\tilde{G}(\tilde{z})|mn - nm \rangle, \quad (17)$$

where  $m$  denotes a state below or above the Fermi surface (continuous choice). The constants  $U_S$  and  $U_V$  are determined from Eqs. (16) and (17). Note that Eq. (10) is an approximation, since the scalar and vector fields are in general momentum dependent.

The energy per nucleon in nuclear matter is

$$\begin{aligned} \frac{\mathcal{E}}{A} &= \frac{1}{A} \sum_{m \leq k_F} \frac{\tilde{M}}{\tilde{E}_m} \langle m|\gamma \cdot \mathbf{p}_m + M|m \rangle \\ &+ \frac{1}{2A} \sum_{m, n \leq k_F} \frac{\tilde{M}^2}{\tilde{E}_m \tilde{E}_n} \langle mn|\tilde{G}(\tilde{z})|mn - nm \rangle - M. \end{aligned} \quad (18)$$

In Eqs. (17) and (18) we use

$$\tilde{z} = \tilde{E}_m + \tilde{E}_n. \quad (19)$$

The expression for the energy, Eq. (18), is denoted by the Dirac-Brueckner-Hartree-Fock (DBHF) approximation. If  $\tilde{M}$  is replaced by  $M$ , we will speak of the Brueckner-Hartree-Fock (BHF) approximation, since this case, qualitatively and quantitatively, corresponds to conventional non-relativistic Brueckner theory. Thus, we will occasionally denote the DBHF calculation by 'relativistic' and the BHF calculation by 'non-relativistic' (though, strictly speaking, all our calculations are relativistic).

In Eqs. (16)–(18) the states  $|m\rangle$  and  $|n\rangle$  are represented by Dirac spinors of the kind Eq. (11) and an appropriate isospin wavefunction,  $\langle m|$  and  $\langle n|$  are the adjoint Dirac spinors  $\tilde{u} = \tilde{u}^\dagger \gamma^0$  with  $\tilde{u}\tilde{u} = 1$ ;  $\tilde{E}_m \equiv \sqrt{\tilde{M}^2 + \mathbf{p}_m^2}$ . The states of the nucleons in nuclear matter,  $w$ , are to be normalized by  $w^\dagger w = 1$ . This is achieved by defining  $w \equiv \sqrt{\tilde{M}/\tilde{E}} \times \tilde{u}$  which explains factors of  $\tilde{M}/\tilde{E}$  in Eqs. (16)–(18).

The first term on the r.h.s. of Eq. (18)—the 'kinetic energy'—is in more explicit form

$$\frac{1}{A} \sum_{m \leq k_F} \frac{M\tilde{M} + \mathbf{p}_m^2}{\tilde{E}_m}. \quad (20)$$

The single particle energy is

$$\epsilon_m = \frac{\tilde{M}}{\tilde{E}_m} \langle m|\gamma \cdot \mathbf{p}_m + M|m \rangle + U(m) \quad (21)$$

$$= \tilde{E}_m + U_V \quad (22)$$

$$= \tilde{E}_m - \tilde{M} + M + U_0. \quad (23)$$

### 3. Results for nuclear matter

We apply now three different OBE potentials to nuclear matter. Our potentials use for  $\pi NN$  the coupling of derivative (pseudovector) type. This is important because the pseudoscalar  $\pi NN$  coupling leads to an unrealistically large attractive medium effect.<sup>8)</sup>

The main difference between the three potentials applied here, is the strength of the tensor force as reflected in the predicted D-state probability of the deuteron,  $P_D$ . With  $P_D = 4.5\%$ , Potential A has the weakest tensor force. Potential B and C predict 5.1% and 5.5%, respectively. It is well-known<sup>8)</sup> that the strength of the tensor force determines the location of the nuclear matter saturation point on the Coester band.<sup>9)</sup> To find out the structure of the Coester band, predictions from more than one potential are needed.

All results presented in this section are obtained either in the Bruckner-Hartree-Fock (BHF) or the Dirac-Brueckner-Hartree-Fock (DBHF) approximation; as mentioned before, occasionally, we will denote these two methods also as the ‘non-relativistic’ and the ‘relativistic’ calculation, respectively.

The repulsive relativistic effect in nuclear matter as created by the DBHF method is shown in Fig. 5.

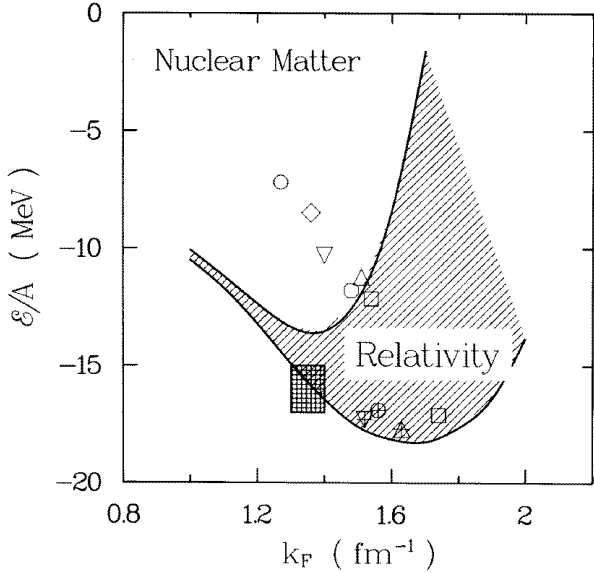


Fig. 5. The repulsive relativistic effect in nuclear matter as obtained in a Dirac-Brueckner-Hartree-Fock calculation using the OBEP-Potential B.<sup>10)</sup> Saturation points from conventional calculations are displayed in the background.<sup>10)</sup> The checked rectangle represents the empirical value for nuclear matter saturation.

As mentioned in Sect. 2, the suppression of the  $\sigma$  contribution can be understood in simple terms by considering the covariant one- $\sigma$ -exchange amplitude, for  $\mathbf{q}' = \mathbf{q}$  and  $\lambda_i = \lambda'_i$  (as used in the Hartree approximation), in which case, due to the covariant normalization of the Dirac spinors, the numerator becomes 1. Since the physical states of the nucleons in nuclear matter,  $w$ , are to be normalized by  $w^\dagger w = 1$  implying  $w \equiv \sqrt{\tilde{M}/\tilde{E}} \times \tilde{u}$ , the sigma (as any other) contribution

gets the (scalar density) factor  $(\tilde{M}/\tilde{E})^2$  (see second term on the r.h.s. of Eq. (18)) which decreases with decreasing  $\tilde{M}$  (i. e. increasing density). A corresponding consideration for the time-like ( $\gamma_0$ ) component of  $\omega$ -exchange would lead to no changes for that contribution. However, due to the exchange term and correlations there is a small enhancement of the repulsion created by the  $\omega$  with density.

It can be shown that the relativistic effect on the energy per nucleon,  $\Delta(\mathcal{E}/A)_{rel}$  (i. e. the difference between the relativistic and non-relativistic calculation), is well fitted by the ansatz

$$\Delta(\mathcal{E}/A)_{rel} \approx 2 \text{ MeV} \times (\rho/\rho_0)^{8/3}, \quad (24)$$

which is suggested by an estimate by Keister and Wiringa.<sup>11)</sup>

Furthermore, we could show that up to nuclear matter density the wound integral  $\kappa$  is slightly smaller for the relativistic approach than for the non-relativistic one.  $\kappa$  can be understood as the expansion parameter for the hole-line series. This implies that in this region the relativistic many-body scheme should be slightly better convergent. Beyond nuclear matter density, the situation is reversed. (For the definition of  $\kappa$  and for explicit formulae appropriate for the momentum-space framework, see section 5 of Ref. 6. In addition, it is amusing to note that for all values of  $k_F$  the ratio  $\tilde{M}/M$  is almost the same for the non-relativistic and the relativistic approach. Low values for  $\tilde{M}/M$  have often been criticized. However, they are not a consequence of the relativistic approach but are due to the Brueckner-Hartree-Fock approximation. Higher order corrections will enhance this quantity.

The representation of nucleons by Dirac spinors with an effective mass,  $\tilde{M}$ , can be interpreted, as taking virtual nucleon-antinucleon excitations in the many-body environment (many-body Z-graphs) effectively into account.<sup>12)</sup> This can be made plausible by expanding the spinors Eq. (11) in terms of (a complete set of) spinor solutions of the free Dirac equation which will necessarily also include solutions representing negative energy (antiparticle) states.

Now let us compare the contributions in various partial-wave states as obtained in a relativistic calculation to that from the corresponding non-relativistic one. Detailed investigations have shown that the repulsive relativistic effect for the  $P$ -wave contributions is essentially due to  $\sigma$  suppression together with a signature of spin-orbit force enhancement. The change of the  $^1S_0$  contribution is so small, because of a cancellation of effects due to  $\sigma$  and  $\rho$ . Apart from  $\sigma$  reduction, the repulsive effect in  $^3S_1$  is due to a suppression of the twice iterated one-pion exchange for reasons quite analogous to the sigma suppression.

A comparison between relativistic and non-relativistic Brueckner-Hartree-Fock calculations for all three potentials is shown in Fig. 6. For the non-relativistic approach, the three saturation points are clearly on the Coester band. However, using the relativistic method, the saturation points are located on a new band which is shifted towards lower Fermi momenta (densities) and even meets the empirical area. This is a very desirable effect. The reason for this shift of the Coester band is the additional strongly density dependent re-

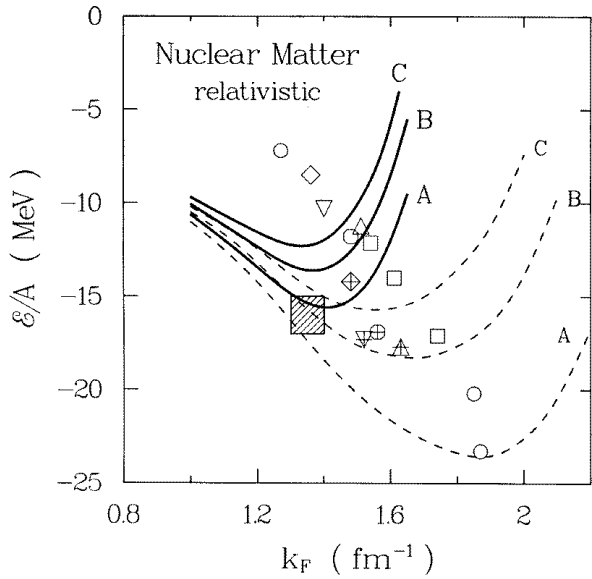


Fig. 6. Results from calculations with a family of relativistic potentials revealing a new Coester band which meets the empirical area;<sup>10)</sup> solid lines: relativistic, dashed lines: non-relativistic calculations. For comparison, saturation points from conventional calculations are displayed in the background.<sup>10)</sup> The shaded square denotes the empirical value for nuclear matter saturation.

pulsion which the relativistic approach gives rise to. In the relativistic case, the incompressibility of nuclear matter using Potential B is about 250 MeV which is in satisfactory agreement with the empirical value of  $210 \pm 30$  MeV.<sup>13)</sup> Note that in the relativistic Walecka model, 540 MeV is obtained for the compression modulus.<sup>14)</sup>

Based on the nuclear matter G-matrix, the effective particle-hole interaction at the Fermi surface is calculated and, multiplied by the density of states  $k_F M / (\hbar^2 \pi^2)$ , parameterized by:  $F = f + f' \tau_1 \cdot \tau_2 + g \sigma_1 \cdot \sigma_2 + g' \sigma_1 \cdot \sigma_2 \tau_1 \cdot \tau_2$ . From an expansion of the parameters in terms of Legendre polynomials,  $P_l$ , we determine the coefficient for  $l = 0$ . It turned out that the prediction for the Landau parameter  $f_0$  is considerably improved in the relativistic calculation without deteriorating the other parameters. Sum rules require  $f_0 > -1$  at nuclear matter density.<sup>7)</sup>

Concerning nuclear matter at higher densities and neutron matter, we like to refer the interested reader to the following Ref. 15.

#### 4. Finite nuclei

Encouraged by the good results for nuclear matter, one may now try to describe finite nuclei starting from the free-space nucleon-nucleon interaction. A straightforward way would be to solve the relativistic Brueckner-Hartree-Fock equations for finite systems. This is, however, an extremely difficult task. Therefore, it might be a reasonable next step to incorporate the DBHF results in a relativistic Hartree framework where the coupling constants are made density dependent so as to reproduce the nuclear matter results.<sup>16)</sup> This relativistic density dependent Hartree (RDDH) approach is similar in spirit to the work by Negele in the nonrelativistic approach.<sup>17)</sup>

The working basis of the RDDH approach for finite nuclei is the relativistic Hartree Lagrangian<sup>18)</sup> (sigma-omega model Lagrangian of Walecka).<sup>19)</sup> Writing explicitly the density dependence of the coupling constants, we have

$$\begin{aligned} \mathcal{L}_{\text{RDDH}} = & \bar{\psi} (i\gamma_\mu \partial^\mu - M - g_\sigma(\rho)\sigma - g_\omega(\rho)\gamma_\mu \omega^\mu) \psi \\ & + \frac{1}{2} (\partial^\mu \sigma)^2 - \frac{1}{2} m_\sigma^2 \sigma^2 - \frac{1}{4} (\partial_\mu \omega_\nu - \partial_\nu \omega_\mu)^2 + \frac{1}{2} m_\omega^2 \omega_\mu^2, \end{aligned} \quad (25)$$

in conventional notation.<sup>4)</sup> In Hartree approximation (mean field approximation), the nucleon self-energy in nuclear matter is given by

$$\Sigma_{\text{RDDH}}(\rho) = U_s(\rho) + U_v(\rho)\gamma_0. \quad (26)$$

Here, the scalar and the vector potentials are expressed in terms of the coupling constants  $g_\sigma(\rho)$  and  $g_\omega(\rho)$  through

$$\begin{aligned} U_s(\rho) &= -\frac{g_\sigma^2(\rho)}{m_\sigma^2} \rho_s, \\ U_v(\rho) &= \frac{g_\omega^2(\rho)}{m_\omega^2} \rho_v, \end{aligned} \quad (27)$$

where  $\rho_s$  and  $\rho_v$  are the scalar and the vector densities, respectively:

$$\begin{aligned} \rho_s &= \langle \bar{\psi} \psi \rangle = 4 \int_0^{k_F} \frac{d^3 k}{(2\pi)^3} \frac{M^*}{E^*}, \\ \rho_v &= \langle \bar{\psi} \gamma_0 \psi \rangle = 4 \int_0^{k_F} \frac{d^3 k}{(2\pi)^3}. \end{aligned} \quad (28)$$

The scalar potential is related to the effective mass by  $M^* = M + U_s(\rho)$ . The connection of the RDDH approach to the DBHF theory is made through the nucleon self-energy in nuclear matter, Eq. (26). In fact, one can express the DBHF self-energy in nuclear matter in this form<sup>20)</sup> using the symmetry requirements and redefinition of various terms through the use of the Dirac equation. The density dependent coupling constants are then obtained through Eqs. (27) and (28), where  $U_s(\rho)$  and  $U_v(\rho)$  are the results of the DBHF calculations of nuclear matter.

We write the equations of motion for finite nuclei for completeness. The normal modes of the nucleon are calculated with the Dirac equation,

$$(-i\boldsymbol{\alpha} \cdot \boldsymbol{\nabla} + \beta M^*(r) + V(r)) \psi_i(\mathbf{r}) = E_i \psi_i(\mathbf{r}), \quad (29)$$

with  $M^*(r) = M + g_\sigma(r)\sigma(r)$  and  $V(r) = g_\omega(r)\omega^0(r) + e \frac{1-\tau_3}{2} A^0(r)$ .

The Klein-Gordon equations for  $\sigma$ ,  $\omega^0$ , and  $A^0$  are

$$\begin{aligned} (-\Delta + m_\sigma^2) \sigma(r) &= -g_\sigma(r)\rho_s(r), \\ (-\Delta + m_\omega^2) \omega^0(r) &= g_\omega(r)\rho_v(r), \\ -\Delta A^0(r) &= e\rho_p(r), \end{aligned} \quad (30)$$

where  $\rho_s$ ,  $\rho_v$  and  $\rho_p$  are the scalar, vector and proton densities, respectively, which are obtained through the Dirac

wavefunctions. We solve the coupled differential equations self-consistently. The center of mass corrections are applied in the same way as in Ref. 21.

In Fig. 7, the vector and the scalar potentials,  $U_v$  and  $U_s$  are depicted as a function of  $k_F$ . At normal matter density,  $k_F = 1.35 \text{ fm}^{-1}$ ,  $U_v = 274.7 \text{ MeV}$  and  $U_s = -355.7 \text{ MeV}$ . As a comparison, the vector and scalar mean-field potentials are shown using constant (density independent) couplings; i.e. the scalar and vector potential parameters are the ones of Potential A. This comparison clearly indicates that one needs density dependent coupling constants in order to reproduce the nuclear matter results within the relativistic Hartree framework.

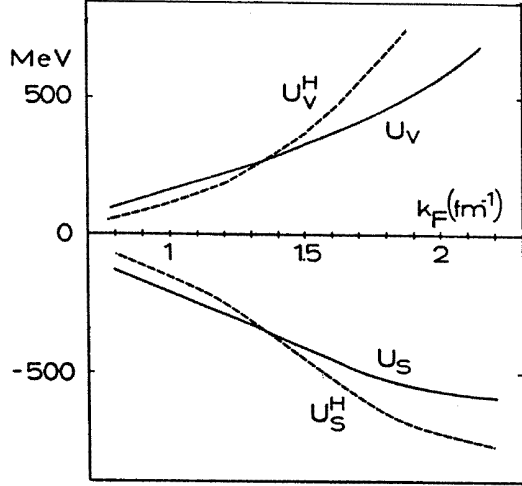


Fig. 7. Vector and scalar potentials for relativistic density dependent Hartree (full lines) and relativistic Hartree only (dashed lines) as a function of  $k_F$ .

Now we fit the coupling constants  $g_\sigma(\rho)$  and  $g_\omega(\rho)$  to the self-energies  $U_s$  and  $U_v$  with the choice that  $m_\sigma$  and  $m_\omega$  are the masses in Potential A as a standard choice;  $m_\sigma = 550 \text{ MeV}$  and  $m_\omega = 782.6 \text{ MeV}$ . As can be seen from Eq. (27), the relevant quantities are  $g_\sigma^2$  and  $g_\omega^2$ . At  $k_F = 0.8, 1.1, 1.5$  we obtain  $g_\sigma^2/4\pi = 12.3, 8.91, 6.23$  and  $g_\omega^2/4\pi = 18.63, 13.48, 9.06$ , respectively. This shows that the coupling constants at the surface are more than 40% bigger than in the interior. At nuclear matter density ( $k_F = 1.35 \text{ fm}^{-1}$ ) the coupling constants are not modified as one can see from Fig. 7. But at smaller densities both coupling constants are growing. We note here that  $U_s$  and  $U_v$  are, in principle, dependent not only on the density but also on the momentum of the nucleon.

We calculate  $^{16}\text{O}$  and  $^{40}\text{Ca}$  as examples for finite nuclei within the RDDH approach. The calculated results on the binding energies, single particle energies and charge radii (using the Bonn A potential) are tabulated in Table 1. For comparison, results of nonrelativistic Brueckner-Hartree-Fock calculations for  $^{16}\text{O}$  with the same potential (Bonn A) are shown in the column N-BHF. It is interesting to find that the RDDH results are very close to experiment. The improvements, as compared to N-BHF, are remarkable. The root mean square charge radius is almost perfect, while the binding energy is slightly smaller than experiment. If we compare relativistic and nonrelativistic results, we find that the radius of the

Table 1. The binding energy per nucleon, root-mean-square charge radius and single particle energies are displayed for the relativistic density dependent Hartree(RDDH) approach, the nonrelativistic Brueckner-Hartree-Fock(N-BHF) method and experiment, respectively. The Bonn A potential is used. The upper part of the table is for  $^{16}\text{O}$  and the lower one for  $^{40}\text{Ca}$ .

$^{16}\text{O}$	RDDH	N-BHF	Experiment
BE/A [MeV]	-7.5	-5.95	-7.98
$r_c$ [fm]	2.66	2.31	$2.70 \pm 0.05$
$\epsilon(1s_{1/2})$ [MeV]	-43.5	-56.6	$-40 \pm 8$
$\epsilon(1p_{3/2})$ [MeV]	-21.8	-25.7	-18.4
$\epsilon(1p_{1/2})$ [MeV]	-16.5	-17.4	-12.1

$^{40}\text{Ca}$	RDDH	N-BHF	Experiment
BE/A [MeV]	-8.0	-8.29	-8.5
$r_c$ [fm]	3.36	2.64	3.5
$\epsilon(1s_{1/2})$ [MeV]	-53.3	-	$-50 \pm 8$
$\epsilon(1p_{3/2})$ [MeV]	-36.0	-	$-34 \pm 5$
$\epsilon(1p_{1/2})$ [MeV]	-32.5	-	$-34 \pm 5$
$\epsilon(1d_{5/2})$ [MeV]	-19.3	-30.2	$-14 \pm 2$
$\epsilon(2s_{1/2})$ [MeV]	-14.3	-24.5	$-10 \pm 1$
$\epsilon(1d_{3/2})$ [MeV]	-13.6	-16.5	$-7 \pm 1$

relativistic calculation is larger. This is natural since, e.g., the lower component of the relativistic  $1p_{3/2}$ -wavefunction looks like a nonrelativistic  $1d_{3/2}$ -wavefunction. This shifts part of the density to the surface and leads to a larger radius in the relativistic case. This has also consequences for the binding energy per nucleon. Using the Bethe-Weizsaecker mass formula, we can estimate that surface and Coulomb effects lead to 2 to 3 MeV less repulsion for the relativistic calculation since the radius is larger. Although the volume effect is 1 to 2 MeV more repulsive in the relativistic case which has been determined in nuclear matter in Ref. 10, the relativistic description of finite nuclei yields altogether more binding energy per nucleon. This shows that relativistic effects lead off the Coester band, which exists for finite nuclei, too.

In Fig. 8, we show a comparison with experimental charge density distributions obtained from elastic electron scattering.<sup>21)</sup> The RDDH results with the Bonn A potential (dash-dotted curve) compare fairly well with the experimental data. Looking more closely, the central density comes out to be higher than experiment and the density falls off slightly faster than experiment. This observation of the density and the slightly smaller binding discussed above, seems to be the reflection of the equation of state of nuclear matter as shown in Fig. 6. In fact, when we take the DBHF results from the Bonn C potential, whose saturation density is almost perfect but the saturation energy is about 4 MeV above the experimental value, the charge density distributions are found to be very good as can be seen in Fig. 8 (dashed curve). In this case, however, the binding energies of finite nuclei are found to be too small; i.e.  $E/A = -5.9 \text{ MeV}$  for  $^{16}\text{O}$  and  $E/A = -6.0 \text{ MeV}$  for  $^{40}\text{Ca}$ .

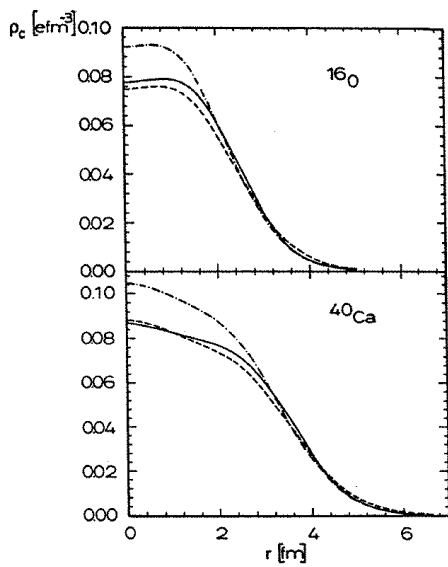


Fig. 8. Comparison of the densities in relativistic density dependent Hartree and experiment for  $^{16}\text{O}$  and  $^{40}\text{Ca}$ , respectively. The results with the Bonn A potential are shown by the dash-dotted curve, while the corresponding ones for Bonn C are depicted by the dashed one.

#### References

- 1) S. Weinberg: Phys. Lett. B **251**, 288 (1990); Nucl. Phys. B **363**, 3 (1991); Phys. Lett. B **295**, 114 (1992).
- 2) D. B. Kaplan, M. J. Savage, and M. B. Wise: Phys. Lett. B **424**, 390 (1998); Nucl. Phys. B **534**, 329 (1998).
- 3) N. Kaiser, R. Brockmann, and W. Weise: Nucl. Phys. A **625**, 758 (1997).
- 4) J. D. Bjorken and S. D. Drell: *Relativistic Quantum Mechanics*, (McGraw-Hill, New York, 1964).
- 5) C. J. Horowitz and B. D. Serot: Nucl. Phys. A **464**, 613 (1987).
- 6) M. I. Haftel and F. Tabakin: Nucl. Phys. A **158**, 1 (1970).
- 7) A. B. Migdal: *Theory of Finite Fermi Systems and Applications to Atomic Nuclei*, (Wiley, New York, 1967).
- 8) R. Machleidt and R. Brockmann: in *Proc. Los Alamos Workshop on Dirac Approaches in Nuclear Physics*, edited by J. R. Shepard et al., LA-10438-C, (Los Alamos, New Mexico, 1985), p. 328.
- 9) F. Coester, S. Cohen, B. D. Day, and C. M. Vincent: Phys. Rev. C **1**, 769 (1970).
- 10) R. Brockmann and R. Machleidt: Phys. Rev. C **42**, 1965 (1990).
- 11) B. Keister and R. B. Wiringa: Phys. Lett. B **173**, 5 (1986).
- 12) G. E. Brown et al.: Comments Nucl. Part. Phys. **17**, 39 (1987).
- 13) J. P. Blaizot: Phys. Rep. **65**, 171 (1980).
- 14) B. D. Serot and J. D. Walecka: Adv. Nucl. Phys. **16**, 1 (1986).
- 15) G. Q. Li, R. Machleidt, and R. Brockmann: Phys. Rev. C **45**, 2782 (1992).
- 16) R. Brockmann and H. Toki: Phys. Rev. Lett. **68**, 3408 (1992).
- 17) J. W. Negele: Phys. Rev. C **1**, 1260 (1970).
- 18) R. Brockmann: Phys. Rev. C **18**, 1510 (1978).
- 19) J. D. Walecka: Ann. Phys. (NY) **83**, 491 (1974).
- 20) R. Brockmann and R. Machleidt: Phys. Lett. B **149**, 283 (1984).
- 21) P. G. Reinhard, M. Rufa, J. Maruhn, W. Greiner, and J. Friedrich: Z. Phys. A **323**, 13 (1986).